

A Study of Interstellar Gas and Stars in the Gravitationally Lensed Galaxy ‘The Cosmic Eye’ from Rest-Frame Ultraviolet Spectroscopy

Anna M. Quider^{1*}, Alice E. Shapley², Max Pettini¹, Charles C. Steidel³, and Daniel P. Stark¹

¹ *Institute of Astronomy, Madingley Rd, Cambridge, CB3 0HA, UK*

² *Department of Physics and Astronomy, University of California, Los Angeles, CA 90095-1547, USA*

³ *California Institute of Technology, Mail Stop 105-24, Pasadena, CA 91125, USA*

Accepted ... Received ... in original form ...

ABSTRACT

We report the results of a study of the rest-frame ultraviolet (UV) spectrum of the Cosmic Eye (J213512.73–010143), a luminous ($L \sim 2L^*$) Lyman break galaxy at $z_{\text{sys}} = 3.07331$ magnified by a factor of ~ 25 via gravitational lensing by foreground mass concentrations at $z = 0.73$ and 0.33 . The spectrum, recorded at high resolution and signal-to-noise ratio with the ESI spectrograph on the Keck II telescope, is rich in absorption features from the gas and massive stars in this galaxy. The interstellar absorption lines are resolved into two components of approximately equal strength and each spanning several hundred km s^{-1} in velocity. One component has a net blueshift of -70 km s^{-1} relative to the stars and H II regions and presumably arises in a galaxy-scale outflow similar to those seen in most star-forming galaxies at $z = 2-3$. The other is more unusual in showing a mean *redshift* of $+350 \text{ km s}^{-1}$ relative to z_{sys} ; possible interpretations include a merging clump, or material ejected by a previous star formation episode and now falling back onto the galaxy, or more simply a chance alignment with a foreground galaxy. In the metal absorption lines, both components only partially cover the OB stars against which they are being viewed. However, there must also be more pervasive diffuse gas to account for the near-total covering fraction of the strong damped Ly α line, indicative of a column density $N(\text{HI}) = (3.0 \pm 0.8) \times 10^{21} \text{ cm}^{-2}$. We tentatively associate this neutral gas with the redshifted component, and propose that it provides the dust ‘foreground screen’ responsible for the low ratio of far-infrared to UV luminosities of the Cosmic Eye.

The C IV P Cygni line in the stellar spectrum is consistent with continuous star formation with a Salpeter initial mass function, stellar masses from 5 to $100 M_{\odot}$, and a metallicity $Z \sim 0.4Z_{\odot}$. Compared to other well-studied examples of strongly lensed galaxies, we find that the young stellar populations of the Cosmic Eye are essentially indistinguishable from those of the Cosmic Horseshoe and MS 1512-cB58. On the other hand, the interstellar spectra of all three galaxies are markedly different, attesting to the real complexity of the interplay between starbursts and ambient interstellar matter in young galaxies observed during the epoch when cosmic star formation was at its peak.

Key words: cosmology: observations — galaxies: evolution — galaxies: starburst — galaxies: individual (Cosmic Eye)

1 INTRODUCTION

High redshift star-forming galaxies are often identified by a break in their ultraviolet continuum that is due to the Lyman limit, partly from interstellar (within the galaxy) and primarily from intergalactic HI absorption below 912 \AA (Steidel et al. 1996). Since the discovery of these ‘Lyman break galaxies’ (or LBGs), samples of galaxies at $z = 2-4$ have increased a thousand-fold. Despite the

variety of methods now employed to select high redshift galaxies, LBGs remain the most common and most extensively studied class of such objects.

Detailed studies of the physical properties of *individual* galaxies have in general been limited by their faintness ($m_{\mathcal{R}}^* = 24.4$, Steidel et al. 1999; Reddy et al. 2008). In a few cases, however, gravitational lensing by foreground massive galaxies, groups, or clusters has afforded rare insights into the stellar populations and interstellar media of galaxies at $z = 2-4$ (e.g. Pettini et al. 2000, 2002; Teplitz et al. 2000; Lemoine-Busserolle et al. 2003; Smail et

* Email: aquider@ast.cam.ac.uk

al. 2007; Swinbank et al. 2007; Cabanac, Valls-Gabaud, & Lidman 2008; Siana et al. 2008, 2009; Finkelstein et al. 2009; Hainline et al. 2009; Quider et al. 2009; Swinbank et al. 2009; Yuan & Kewley 2009 and references therein). The order-of-magnitude boost in flux provided by strong lensing makes it possible to record the spectra of these galaxies with a combination of high resolution and high signal-to-noise ratio (S/N) which for normal, unlensed galaxies will have to wait until the next generation of 30+ m optical/infrared telescopes.

Focusing on the rest-frame UV spectra in particular, our group has so far published observations of two of these strongly lensed high redshift galaxies: MS 1512-cB58 and J1148+1930 (cB58 and the ‘Cosmic Horseshoe’ respectively; Pettini et al. 2002; Quider et al. 2009). Both are $\sim L^*$ galaxies at redshifts $z \sim 2.5$ magnified by a factor of ~ 30 (Seitz et al. 1998; Dye et al. 2008). A considerable amount of data that are inaccessible to typical low-resolution studies is contained in these rest-UV spectra, including information on interstellar gas composition and kinematics, on the initial mass function (IMF) of starbursts at high z , and clues to the geometry of the gas and stars.

One of the motivations for this work is to assess the range of properties possessed by high redshift star-forming galaxies. By comparing the UV spectra of cB58 and the Cosmic Horseshoe, Quider et al. (2009) showed that the young stellar populations of these galaxies are very similar, as are the metallicities and kinematics of their interstellar media. On the other hand, the two galaxies exhibit clear differences in the covering fractions of their stars by the interstellar gas, differences which are reflected in the strikingly different morphologies of their Lyman α lines (a damped absorption profile in cB58 and a double-peaked emission profile in the Horseshoe). Studies at other wavelengths (Teplitz et al. 2000; Hainline et al. 2009) have also shown that cB58 and the Cosmic Horseshoe have comparable star formation rates, $\text{SFR} \sim 50\text{--}100 M_{\odot} \text{ yr}^{-1}$, at the upper end of the range of values measured in star-forming galaxies at $z = 2\text{--}3$, and similar dynamical masses, $M_{\text{dyn}} \sim 1 \times 10^{10} M_{\odot}$, typical of luminous galaxies at this epoch (Pettini et al. 2001; Erb et al. 2006b,c; Reddy et al. 2006).

Clearly, several examples of strongly lensed galaxies need to be studied at such levels of detail for a full characterization of galaxy properties at these redshifts. Fortunately, many new cases have been discovered recently, mostly from dedicated searches in imaging data from the Sloan Digital Sky Survey (Estrada et al. 2007; Belokurov et al. 2007, 2009; Ofek et al. 2008; Shin et al. 2008; Kubo et al. 2009; Lin et al. 2009; Wen et al. 2009). Other surveys have capitalised on the superior spatial resolution of *Hubble Space Telescope* (*HST*) to identify high redshift galaxies strongly lensed into multiple images or arcs; the $z = 3.0733$ galaxy which is the focus of the present paper, dubbed the ‘Cosmic Eye’, was indeed discovered by Smail et al. (2007) from an *HST* Snapshot program targeting high luminosity X-ray clusters.

In this paper we present high resolution observations of the rest-frame UV spectrum of the Cosmic Eye. The paper is organized as follows. In Section 2 we summarize the known properties of the Cosmic Eye from previous studies at a variety of wavelengths, while Section 3 has details of our observations and data reduction. We analyze the interstellar spectrum of the Cosmic Eye in Section 4, and the composite spectrum of its young stellar population in Section 5. Section 6 focuses on the numerous intervening absorption systems that potentially confound our interpretation of the galaxy’s intrinsic features. In Section 7 we discuss the implications of our findings; finally, we summarize our main conclusions

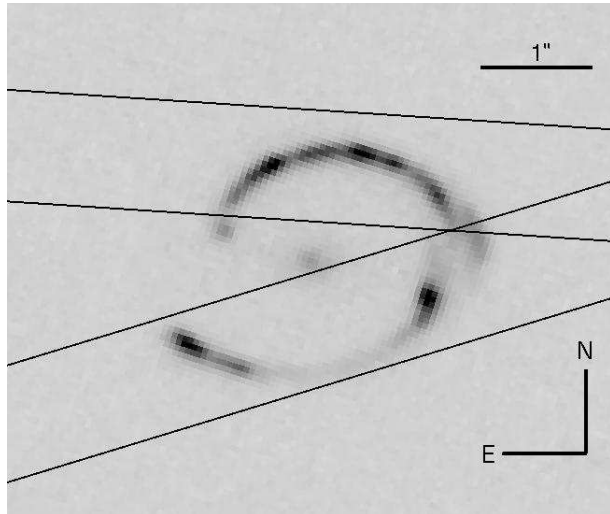


Figure 1. HST/ACS F606W image of the Cosmic Eye. The straight lines indicate the two placements of the $1.0 \times 20''$ entrance slit of ESI used for the observations reported here.

in Section 8. Throughout the paper, we adopt a cosmology with $\Omega_{\text{M}} = 0.3$, $\Omega_{\Lambda} = 0.7$, and $H_0 = 70 \text{ km s}^{-1} \text{ Mpc}^{-1}$.

2 THE COSMIC EYE

Among the bright, strongly lensed, high redshift galaxies, the Cosmic Eye is the most well-studied to date after cB58. Here we summarize available information which is relevant to our analysis.

The Cosmic Eye, also known as LBG J213512.73–010143, was so named because it consists of two bright arcs extending $\sim 3''$ which nearly fully surround a compact galaxy (Figure 1). From low resolution spectroscopy, the central galaxy was classified as a massive early-type spiral, or S0, galaxy at $z = 0.73$, and from rest-frame optical spectroscopy the source redshift was estimated to be $z = 3.0743$ (Smail et al. 2007). The detailed lensing model by Dye et al. (2007) concluded that the lensing of the Cosmic Eye is attributable to both the galaxy at $z = 0.73$ and a foreground cluster, MACS J2135.2-0102, at $z = 0.33$. Their models require two source components at similar redshifts: a main component which creates the Eye’s ringed structure, and a secondary component, offset $\sim 0.3''$ to the west, responsible for producing faint extensions at either end of the northern arc. The total magnification of the system is estimated to be ~ 25 ; when this is taken into account, the observed magnitude $r = 20.3$ corresponds to an intrinsic luminosity $L_{1700} \sim 1.5\text{--}2L_{1700}^*$ compared to the luminosity function of $z = 3$ galaxies estimated by Steidel et al. (1999) and more recently Reddy et al. (2008).

The geometry and kinematics of the Cosmic Eye have begun to be explored. Most recently, Siana et al. (2009) used the galaxy’s far-infrared luminosity, which they found to be ~ 8 times lower than expected from its rest-frame UV luminosity, to argue that a reddening curve similar to those determined from observations of stars in the Large and Small Magellanic Clouds (LMC/SMC) is more appropriate for the dust in the Cosmic Eye than the Calzetti et al. (2000) attenuation curve normally adopted for starbursts. The difference between the two reddening laws is one of geometry: the Calzetti et al. (2000) curve is thought to arise from a configuration where stars and dust are mixed together, whereas the LMC/SMC

(or, for that matter, Milky Way) extinction curves are more appropriate to the reddening produced by a ‘screen of dust’ which is in the foreground of the sources of UV light.

Integral field spectroscopy of $H\beta$ and $[O\text{III}]\lambda\lambda 4959, 5007$ nebular emission lines with the OH-Suppressing Infrared Integral Field Spectrograph (OSIRIS) on the Keck II telescope (Stark et al. 2008) showed a regular rotation pattern $v_{\text{rot}} \sin i = 55 \text{ km s}^{-1}$ on which are superimposed random motions with a comparable velocity dispersion of $\sigma = 54 \text{ km s}^{-1}$. Coppin et al. (2007) detected CO emission from the Cosmic Eye and found the signal to peak at the location of the secondary component of the source, suggesting that this component may be the remaining reservoir of gas available to fuel star formation.

The star formation rate of the galaxy has been estimated from its luminosity in the UV stellar continuum, $H\beta$ emission line, and infrared dust emission to be $\text{SFR} \sim 100, \sim 100, \text{ and } \sim 60 - 140 M_{\odot} \text{ yr}^{-1}$, respectively (Smail et al. 2007; Stark et al. 2008; Coppin et al. 2007; Siana et al. 2009).¹ The metallicity determined from the ratio of strong emission lines (the R_{23} method of Pagel et al. 1979), is $Z \sim 0.9 Z_{\odot}$ (Stark et al. 2008). At the current rate of star formation, it would have taken the galaxy $\sim 100 \text{ Myr}$ to build its stellar mass of $\sim 6 \times 10^9 M_{\odot}$ (Coppin et al. 2007).

To this growing body of data we now add a high resolution study of the rest-frame UV spectrum of the Cosmic Eye. At UV wavelengths the spectrum is dominated by the combined emission from early-type stars and absorption from interstellar gas. Such data can shed new light on the kinematics, chemical composition and stellar populations of this galaxy, complementing the information gleaned from other wavelengths.

3 OBSERVATIONS AND DATA REDUCTION

The procedures we followed for our observations and data reduction were very similar to those described by Quider et al. (2009) in their study of the Cosmic Horseshoe, and we refer the interested reader to that paper for a comprehensive account. Briefly, we used the Echellette Spectrograph and Imager (ESI; Sheinis et al. 2000) on the Keck II telescope to record the rest-frame UV spectrum of the Cosmic Eye on the nights of 2007 September 13 and 14 UT. With its high efficiency, wide wavelength coverage (from ~ 4000 to $10\,000 \text{ \AA}$), and moderately high resolution ($R \equiv \lambda/\Delta\lambda = 4000$), ESI is the instrument of choice for this work. On the first night, the $1''$ wide slit of ESI was positioned on the northern arc of the Cosmic Eye at position angle P.A. = 86.44° (see Figure 1); on the second night we recorded the light of the southern arc at P.A. = 287.12° . The total exposure time for each arc was 16 000 s, broken up into eight 2000 s long integrations on the ESI detector. The seeing was sub-arcsecond on both nights.

Inspection of the two-dimensional (2D) spectra shows that only the light from the main ring structure was recorded; the fainter extensions to the east and the west of the northern ring which, as explained above (Section 2), are due to the secondary component of the source in the lensing model of Dye et al. (2007), were only partially covered by the slit placements (see Figure 1) and are in any case much fainter than the main ring structures.

¹ All of these estimates are based on the conversion factors between luminosity and SFR given by Kennicutt (1998) and are appropriate for a Salpeter (1955) IMF. Adoption of a more realistic formulation of the IMF, such as that proposed by Chabrier (2003), would result in smaller values of SFR by a factor of 1.8.

Table 1. SYSTEMIC REDSHIFT

Ion	$\lambda_{\text{lab}}^{\text{a}}$ (\AA)	z	Origin
C II+N III	1324.1418 ^b	3.0731	Stars
O IV	1343.354	3.0730	Stars
S V	1501.763	3.0732	Stars
$H\beta^{\text{c}}$	4862.721	3.0737	H II Regions
$[O\text{III}]^{\text{c}}$	4960.295	3.0734	H II Regions
$[O\text{III}]^{\text{c}}$	5008.239	3.0735	H II Regions

^a Vacuum wavelengths.

^b Central wavelength of the blend.

^c Measured from OSIRIS data reported by Stark et al. (2008).

The data were processed with standard IRAF tasks following the steps outlined in Quider et al. (2009); compared to that work, subtraction of the background was considerably more straightforward because in the present case light from the lensing galaxy did not fall within the ESI slit (see Figure 1). Nevertheless, once the data were fully reduced as described below, we found residual flux in the core of the damped $\text{Ly}\alpha$ absorption line (see Section 4.4), amounting to $\sim 5\%$ of the continuum level. We cannot determine whether the effect is real, indicating that the damped $\text{Ly}\alpha$ line only covers 95% of the OB stars producing the continuum near 1216 \AA , or is an artifact of errors in the determination of the background level to be subtracted. Nor do we have any other ‘markers’ in the spectrum as definitive as the damped $\text{Ly}\alpha$ line to help us assess whether this background correction, whatever its origin, is constant along the spectrum or varies with wavelength. In the circumstances, we limited ourselves to applying to the final one-dimensional (1D) spectrum a uniform background correction of 5% of the continuum flux.

At the S/N ratio of the present data, we could not find any significant differences between the extracted 1D spectra of the northern and southern arcs; their similarity is consistent with the lensing model of Dye et al. (2007) which shows them to be images of the same source, mostly contained within the caustic (see Figure 4 of Dye et al. 2007).² Therefore, we averaged the spectra of the two arcs and rebinned the resulting spectrum to 0.5 \AA bins to maximise the S/N ratio. The final composite 1D spectrum has an average $S/N \simeq 14$ per 0.5 \AA bin between 5200 and 7500 \AA (1275 – 1840 \AA in the rest-frame of the source), and a resolution $\text{FWHM} = 75 \text{ km s}^{-1}$, sampled with ~ 3 wavelength bins.

4 THE INTERSTELLAR SPECTRUM

4.1 The systemic redshift of the Cosmic Eye

An accurate determination of the systemic redshift of the lensed galaxy in the Cosmic Eye is critical to the rest of our analysis. Our rest-frame UV spectrum includes several absorption features from the photospheres of hot stars which can be used for this purpose. The cleanest among these are O IV $\lambda 1343.354$, S V $\lambda 1501.763$, and

² Note, however, that Smail et al. (2007) did report differences in the profiles of the interstellar absorption lines between the northern and southern arcs. The fact that we do not confirm such differences could be due either to the higher S/N ratio and resolution of our spectra, or to the different slit positions employed in the two studies.

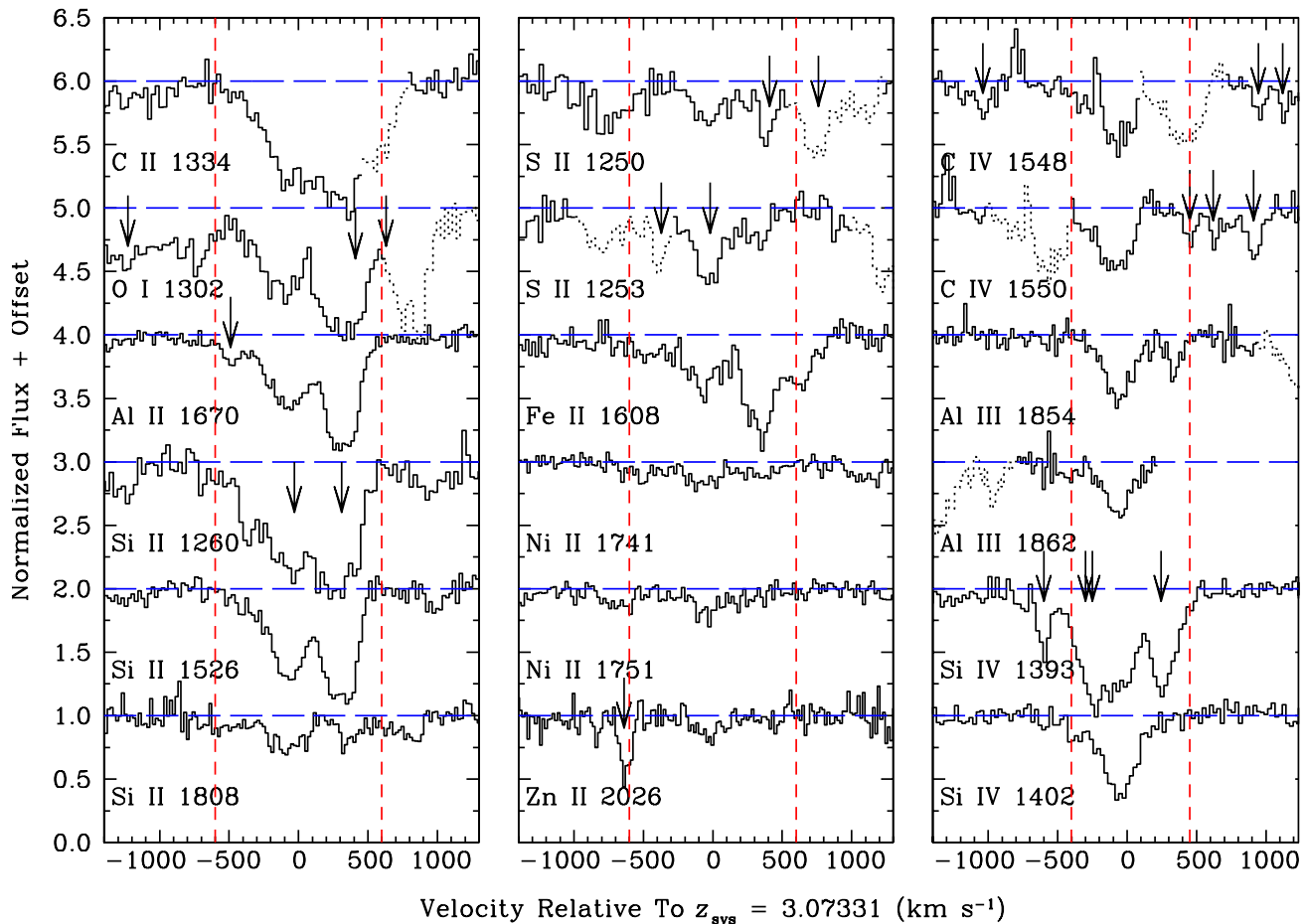


Figure 2. Normalized profiles of selected interstellar absorption lines. *Left and middle panels:* Transitions of ions which are dominant in H I regions. *Right panel:* Transitions of ions which are ionized beyond the species dominant in H I regions. The vertical red dash lines indicate the velocity range over which we measured the equivalent widths of the strongest absorption lines (see Table 2). Arrows mark the locations of intervening absorption lines unrelated to the Cosmic Eye; these are sometimes resolved as individual features (e.g. see panel for Zn II λ 2026), while in other cases they add to absorption from the Cosmic Eye (e.g. see panel for Si II λ 1260). Section 6 and Table 3 give a full account of these intervening absorption systems.

a close blend of C II and N III lines centred at λ 1324.1418 (all vacuum wavelengths). Table 1 lists the redshifts deduced from each of these stellar lines, as well as the values of redshift we measured from the H β and [O III] $\lambda\lambda$ 4959, 5007 emission lines in the OSIRIS spectrum of Stark et al. (2008). As can be seen from Table 1, the mean redshift of the UV stellar lines, $\langle z_{\text{OB stars}} \rangle = 3.0731$, differs by -29 km s^{-1} from the mean $\langle z_{\text{H II}} \rangle = 3.0735$ of the three nebular lines.³ This small difference may reflect a small offset between the wavelength calibrations of ESI and OSIRIS, or may be simply due to noise in the spectra. It could also be real but, as we have no other reason to suspect that the massive stars in this galaxy and the nebulae they ionize should be at systematically different redshifts, we decided to average together all the values of redshift in Table 1 to deduce a mean systemic redshift for the galaxy $z_{\text{sys}} = 3.07331 \pm 0.00024$ (1σ). The standard deviation corresponds to a velocity uncertainty $\delta v = 18 \text{ km s}^{-1}$, or just over one half of a wavelength bin in the final 1D ESI spectrum.

³ Note that this differs from $\langle z_{\text{H II}} \rangle = 3.0743$ reported by Smail et al. (2007), but the latter is now thought to have been incorrectly estimated (M. Swinbank, private communication).

4.2 Kinematics of the absorbing gas

We closely inspected the spectrum of the Cosmic Eye for interstellar absorption lines and identified 20 transitions from eight elements in different ionization states, from O I to C IV. The absorption lines are listed in Table 2 and all but two (for clarity purposes) are reproduced in the montage in Figure 2.

The most striking aspect of the Cosmic Eye’s interstellar absorption lines is that they consist of two distinct components: a (mostly) blueshifted component centred at $v_{\text{blue}} \simeq -70 \text{ km s}^{-1}$ relative to $z_{\text{sys}} = 3.07331$, and a redshifted component centred at $v_{\text{red}} \simeq +350 \text{ km s}^{-1}$ (these velocities refer to the wavelength bins with the highest apparent optical depth in the line profiles).

As we shall see below (Section 6), the sightline to the Cosmic Eye intersects several lower redshift absorbers that produce a multitude of intervening absorption lines unrelated to the lensed galaxy at $z = 3.07331$. These features do complicate the interpretation of the interstellar absorption due to the Cosmic Eye itself; in Figure 2 we have indicated with downward pointing arrows instances where the absorption lines due to the interstellar medium in the Cosmic Eye are contaminated by intervening absorbers at

Table 2. INTERSTELLAR ABSORPTION LINES

Ion	$\lambda_{\text{lab}}^{\text{a}}$ (Å)	f^{a}	$\Delta v_{\text{blue}}^{\text{b}}$ (km s ⁻¹)	$z_{\text{blue}}^{\text{c}}$	$W_{\text{blue}}^{\text{d}}$ (Å)	$\delta W_{\text{blue}}^{\text{e}}$ (Å)	$\Delta v_{\text{red}}^{\text{f}}$ (km s ⁻¹)	$z_{\text{red}}^{\text{g}}$	$W_{\text{red}}^{\text{h}}$ (Å)	$\delta W_{\text{red}}^{\text{i}}$ (Å)	Comments
(1)	(2)	(3)	(4)	(5)	(6)	(7)	(8)	(9)	(10)	(11)	(12)
C II	1334.5323	0.1278	-600, +600 ^j	3.0752 ^j	3.15 ^j	0.06 ^j	Blended with C II* λ 1335.6627
C IV	1548.204	0.1899	-400, +100	3.0719	0.68	0.06	Blended with stellar C IV λ 1549.1
	1550.781	0.09475	-400, +100	3.0718	0.74	0.04	Blended with stellar C IV λ 1549.1
O I	1302.1685	0.04887	-500, +75	3.0711	1.12	0.04	Redshifted component blended with Si II λ 1304.3702
Al II	1670.7886	1.74	-400, +150	3.0722	1.19	0.02	+150, +600	3.0777	1.40	0.02	
Al III	1854.7184	0.559	-400, +200	3.0725	0.84	0.02	+200, +450	3.0779	0.23	0.01	
	1862.7910	0.278	-400, +180	3.0722	0.68	0.02	
Si II	1260.4221	1.18	-600, +600 ^j	3.0740 ^j	3.20 ^j	0.05 ^j	Blended with Si II λ 1259.519
	1304.3702	0.0863	+85, +500	3.0772	1.20	0.03	Blueshifted component blended with O I λ 1302.1685
	1526.7070	0.133	-600, +100	3.0716	1.22	0.03	+100, +600	3.0772	1.30	0.02	
	1808.0129	0.00208	-300, +150	3.0723	0.48	0.03	+150, +500	3.0782	0.24	0.03	
Si IV	1393.7602	0.513	-500, +120	3.0711	1.83	0.03	
	1402.7729	0.254	-400, +200	3.0722	0.94	0.03	
S II	1250.578	0.00543	-300, +150	3.0727	0.45	0.03	+150, +500	3.0780	0.40	0.03	
	1253.805	0.0109	-300, +150	3.0726	0.69	0.03	+150, +500	3.0774	0.28	0.03	
Fe II	1608.4511	0.0577	-300, +150	3.0724	0.69	0.03	+150, +500	3.0779	1.03	0.03	
Ni II	1709.6042	0.0324	-300, +150	3.0727	0.17	0.02	+150, +500	3.0775	0.15	0.02	
	1741.5531	0.0427	-300, +150	3.0724	0.31	0.03	+150, +500	3.0777	0.18	0.02	
	1751.9157	0.0277	-300, +150	3.0726	0.31	0.03	+150, +500	3.0769	0.12	0.02	
Zn II	2026.137	0.501	-300, +150	3.0729	0.27	0.03	+150, +500	3.0783	0.12	0.02	

^a Vacuum wavelength and f -values are from Morton (2003) with updates by Jenkins & Tripp (2006).

^b Velocity range for measurements of blueshifted absorption component.

^c Redshift of the centroid of blueshifted absorption component.

^d Rest-frame equivalent width of blueshifted absorption component.

^e 1σ random error on the rest-frame equivalent width of blueshifted absorption component.

^f Velocity range for measurements of redshifted absorption component.

^g Redshift of the centroid of redshifted absorption component.

^h Rest-frame equivalent width of redshifted absorption component.

ⁱ 1σ random error on the rest-frame equivalent width of redshifted absorption component.

^j These values refer to the blend of blueshifted and redshifted absorption components.

lower redshifts. The two-component structure of the interstellar lines in the Cosmic Eye is most clearly seen in Figure 2 in unblended transitions recorded at high S/N, such as Si II λ 1526.7070 and Al II λ 1670.7886. From these absorption lines it appears that the blueshifted component extends over a velocity range $\Delta v \sim 700$ km s⁻¹, from ~ -600 km s⁻¹ to $\sim +100$ km s⁻¹ relative to the systemic redshift $z_{\text{sys}} = 3.07331$, while the redshifted component is somewhat narrower with $\Delta v \sim 500$ km s⁻¹ (from $\sim +100$ km s⁻¹ to $\sim +600$ km s⁻¹ relative to z_{sys}). Furthermore, it can be seen from Figure 2 that the redshifted component is absent in the absorption lines of the most highly ionized gas, C IV and Si IV, and is relatively weak in the intermediate ionization stage Al III. Whenever possible, we have listed measurements of absorption redshift and equivalent width separately for the two components in Table 2. Note, however, that the values of equivalent width given in the table may include blends with intervening absorption features, as explained above; in this respect, the purely random errors quoted in columns (7) and (11) underestimate the true uncertainties (random and systematic) affecting these measurements.

The kinematic pattern revealed by Figure 2 is unexpected for star-forming galaxies at all redshifts, where the interstellar medium seen in absorption against the starburst is primarily moving with *negative* velocities, commonly interpreted as large-scale outflows.

For example, in the stack of more than 800 low resolution spectra of galaxies at $z \simeq 3$ constructed by Shapley et al. (2003), the interstellar lines have a net blueshift of ~ -150 km s⁻¹, and an analogous result is found in stacked spectra of galaxies at $z = 2$ (Law et al. 2007), and $z = 4, 5$ and 6 (Vanzella et al. 2009). Similarly, in her ESI study of the interstellar Na I D lines in 18 local ultraluminous infrared galaxies, Martin (2005) found signatures of outflows in 15 cases and of inflow in only one case. Our earlier high-resolution work on other strongly lensed galaxies at $z = 2 - 3$ (Pettini et al. 2002; Quider et al. 2009) did show a tail of absorption extending to positive velocities, but what we see in the Cosmic Eye is qualitatively different, with the redshifted component being of comparable strength to the blueshifted absorption. When observed at the low resolutions of most spectra of high- z galaxies ($R < 1000$), the stronger interstellar lines in the Cosmic Eye would have a net redshift of $\sim +150$ km s⁻¹, which is highly unusual (e.g. Steidel et al. in preparation). We discuss possible interpretations in Section 7.2.

4.3 Partial Coverage

The profiles of the interstellar lines in the Cosmic Eye hold clues to the geometry of gas, dust, and stars in this galaxy. An inspection of Figure 2 reveals that the cores of the strongest lines which are

not contaminated by intervening absorption at lower redshifts (that is, lines not marked by a downward pointing arrow) do not reach zero flux in either of the two kinematic components. We consider the implications of this residual intensity in the line cores for each component in turn.

First we consider the redshifted component. Si II $\lambda 1526$, Al II $\lambda 1670$ and Fe II $\lambda 1608$ all exhibit flat cores at a residual intensity of $I_\lambda/I_0 \simeq 0.15$ (where I_λ is the measured intensity in the line at wavelength λ and I_0 is intensity in the continuum). The most straightforward interpretation is that we are seeing the superposition within the spectrum of saturated absorption lines and escaping continuum photons. Such a scenario would apply if the absorbing material only covers $\sim 85\%$ of the continuum source.

The analysis of the blueshifted component is less clear-cut. It appears to be covering even less of the stellar light than the redshifted component, with the saturated cores of Si II $\lambda 1526$ and O I $\lambda 1302$ levelling at a residual intensity $I_\lambda/I_0 \simeq 0.3$, corresponding to an apparent optical depth $\tau_a \sim 1$ [with the usual definition of the optical depth τ given by $I_\lambda/I_0 = \exp(-\tau)$]. Al II $\lambda 1670$ and Fe II $\lambda 1608$ may not be fully saturated in this component, since their minimum residual intensities (in the blue component) are higher: $I_\lambda/I_0 \simeq 0.45$, and $\simeq 0.55$ respectively. On the other hand, we do not have a satisfactory explanation for the higher apparent optical depth of C II $\lambda 1334$, unless this transition is blended with other unrecognized absorption (in addition to the fine structure line C II* $\lambda 1335$ which would fall $\sim 250 \text{ km s}^{-1}$ to the red in the top left-hand panel of Figure 2).

In any case, a lower covering factor of the blueshifted gas compared to the redshifted absorption is required in order to make sense of the apparent contradiction between the relative strengths of the red and blue components in absorption lines of differing f -values. For example, the two components are observed to have comparable values of τ_a in Si II $\lambda 1808$ but different values in Si II $\lambda 1526$, with the blue component being weaker than the red one (see lower two panels in the left-hand column of Figure 2). Such an arrangement would at first sight appear to be unphysical. These two Si II transitions have widely different f -values (see Table 2); since they both arise from the same ground state of Si⁺, their *intrinsic* optical depths must be in the same ratio as their $\lambda \times f$ products, or $\tau(1526)/\tau(1808) = 54$. This expectation can only be reconciled with the measured values of *apparent* optical depth, τ_a , if we assume that the covering factor of the blue component is lower than that of the red one, and that both components are in fact saturated in Si II $\lambda 1526$. Once that is taken into account, and the zero level adjusted accordingly, the intrinsic (rather than apparent) optical depth is actually higher in the blue component than in the red one.

The combination of: (a) partial coverage by differing factors for the blue and red components, and possibly even varying as a function of velocity within each component (see Martin & Bouché 2009); (b) contamination by unrelated absorption features due to lower redshift systems; and (c) limited S/N ratio, makes it very difficult in our view to deduce reliable ion column densities from the analysis of the line profiles. Accordingly, we have refrained from attempting to do so.

4.4 The Lyman α line

The Ly α line in the Cosmic Eye shows a strong damped absorption profile, from which we deduce a neutral hydrogen column density $N(\text{H I}) = (3.0 \pm 0.8) \times 10^{21} \text{ cm}^{-2}$ (see Figure 3). This is a high value of $N(\text{H I})$, near the upper end of the column density distribution of QSO-DLAs (Noterdaeme et al. 2009) and more typical

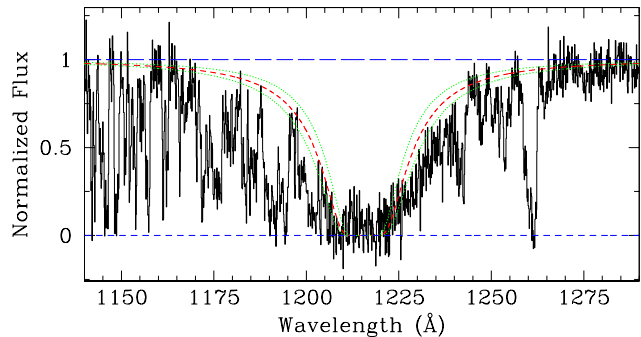


Figure 3. Portion of the ESI spectrum of the lensed galaxy in the Cosmic Eye encompassing the region of the Ly α line. Overlaid on the spectrum are three theoretical damped profiles, centred at $z_{\text{sys}} = 3.07331$, produced by column densities of neutral hydrogen $N(\text{H I}) = (3.0 \pm 0.8) \times 10^{21} \text{ cm}^{-2}$.

of the DLAs seen in the spectra of the afterglows of high redshift gamma-ray bursts (Pontzen et al. 2010). The corresponding line width is $\text{FWHM} = 27.4 \text{ \AA}$ or $\sim 6750 \text{ km s}^{-1}$ (Jenkins 1971). On kinematic grounds it is therefore impossible, with the S/N ratio of the present data, to assign the DLA absorption to one or other of the two main components visible in the metal absorption lines, which are separated by only $\approx 400 \text{ km s}^{-1}$ (Section 4.2).

Nevertheless, we suspect that most of the DLA absorption may be due to the redshifted component, which has the larger covering fraction of the two and consists primarily of neutral gas. The $\sim 70\%$ covering factor we surmised for the outflowing, blueshifted, component may lead to the escape of a substantial fraction of the Ly α photons produced by the H II regions surrounding the OB stars, as found by Quider et al. (2009) in the case of the Cosmic Horseshoe. And yet no Ly α emission line is seen here, not even as residual emission when the damped profile is divided out, as is the case in cB58 (Pettini et al. 2000, 2002) and in the lensed $z = 3.77$ LBG FORJ0332–3557 observed by Cabanac et al. (2008). It is possible that any Ly α photons that escape from the star-forming regions in the Cosmic Eye are absorbed by the foreground neutral gas giving rise to the redshifted component of the metal absorption lines.

It is interesting that the damped Ly α line has a larger covering factor than any other absorption feature in the spectrum. Recall that at the outset we subtracted off 5% of the continuum flux from the entire spectrum (Section 3), in order to bring the core of the damped Ly α line to zero. At this small level, we cannot be sure whether this residual flux in the core of the line is due to inaccurate background estimation, or is the true level of unobscured continuum flux. In any case, the correction we have applied to our data translates to a lower limit of 95% to the covering factor of the OB star continuum by foreground H I gas. The fact that this is larger than the values we deduced in Section 4.3 for the metal lines is not surprising, given that for solar abundances the optical depth in the Ly α line will exceed that of even the strongest metal lines from H I regions by factors of $> 10^4$. In other words, low column densities of gas, undetectable even in the strongest metal absorption lines, could be adding to the apparent optical depth in Ly α to give a higher overall covering fraction.

Bringing together the points discussed in this Section, our high resolution ESI observations have revealed that the interstellar spectrum of the Cosmic Eye is unusual in showing two absorption components, of approximately equal strengths, one blueshifted by -70 km s^{-1} and the other redshifted by $+350 \text{ km s}^{-1}$ relative

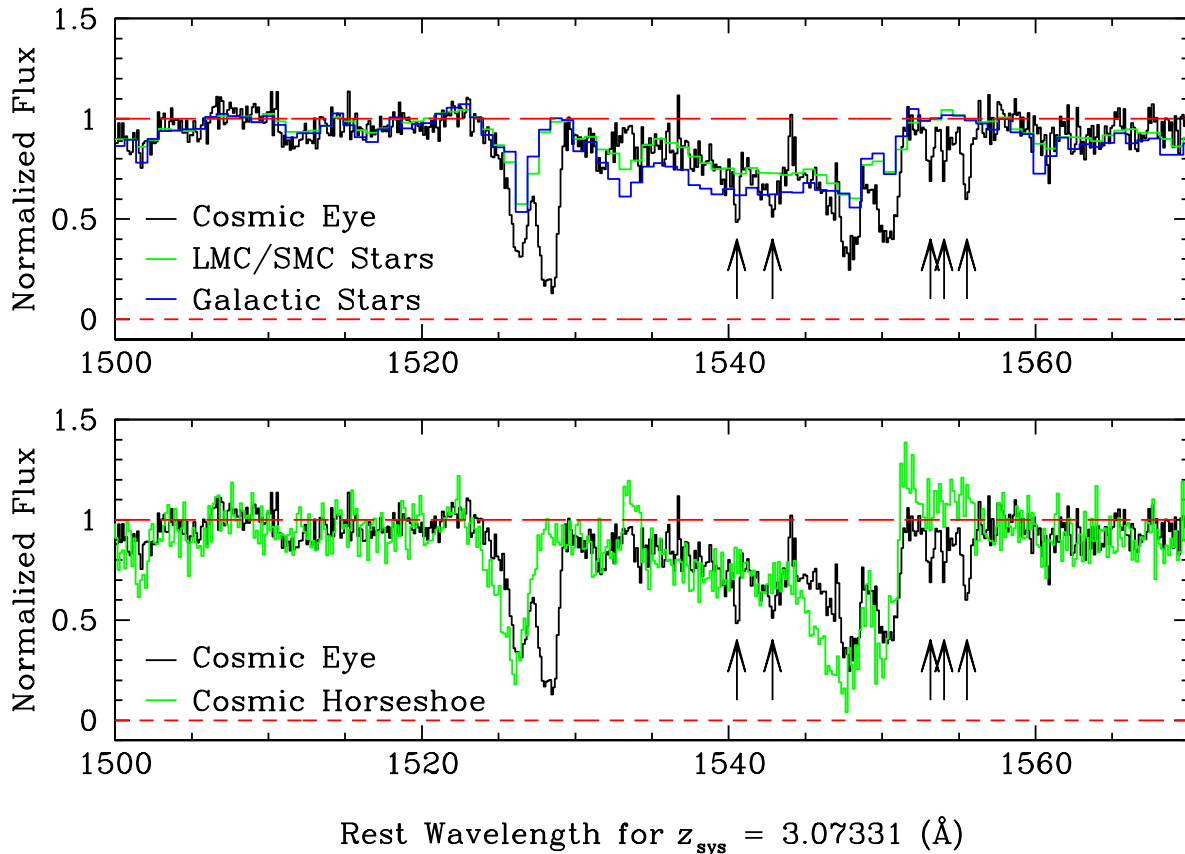


Figure 4. *Upper panel:* Comparison between the ESI spectrum of the Cosmic Eye in the region encompassing the C IV line and model spectra computed with *Starburst99* and empirical libraries of Galactic and Magellanic Clouds stars, as indicated. The model spectra were generated assuming a 100 Myr old continuous star formation episode with a Salpeter IMF with an upper mass limit $M_{\text{up}} = 100M_{\odot}$. *Lower panel:* The stellar spectra of the Cosmic Eye and of the Cosmic Horseshoe are remarkably similar in the wavelength region shown. The ESI spectrum of the Cosmic Horseshoe is reproduced from Quider et al. (2009), and has been reduced to its rest wavelengths at $z_{\text{stars}} = 2.38115$. Upward pointing arrows indicate the positions of narrow, intervening absorption lines unrelated to the Cosmic Eye itself (see Section 6): a possible C IV doublet and three closely spaced Al II $\lambda 1670$ lines.

to the systemic redshift $z_{\text{sys}} = 3.07331$ defined by the OB stars and their H II regions. The redshifted component is mostly of low ionization. The interpretation of the interstellar spectrum is complicated by the fact that the metal lines appear to only partially cover the starburst, with differing covering factors for blueshifted and redshifted absorption. There is a very large column of foreground neutral gas, $N(\text{H I}) = 3 \times 10^{21} \text{ cm}^{-2}$, giving rise to a strong damped Ly α line which covers at least 95% of the stellar continuum.

5 THE STELLAR SPECTRUM

The stars which provide the rest-frame UV continuum light in a high redshift galaxy leave their imprint on the galaxy’s spectrum. The stellar wind features are a clear signature from the most massive O stars which have the strongest stellar winds (Kudritzki & Puls 2000). Rix et al. (2004) have shown that the P Cygni profile of the stellar wind features is sensitive to the metallicity of the stars, as well as to the slope and upper mass cut-off of the IMF. While stellar and interstellar features are usually blended at the low resolution of typical high redshift galaxy spectra (Crowther et al. 2006), the high

resolution of our spectrum allows us to easily separate them and focus on the stellar component.

We used model spectra computed with the spectral synthesis code *Starburst99* to exploit the metallicity and IMF sensitivities of the P Cygni profiles evident in the spectrum of the Cosmic Eye. The two model spectra considered here were generated using libraries of empirical UV spectra from stars either within the Galaxy ($Z \sim 1.0 Z_{\odot}$), or within the Large and Small Magellanic Clouds ($Z \sim 0.4 Z_{\odot}$; Leitherer et al. 1999, 2001). Both models are for 100 Myr old continuous star formation with a Salpeter IMF with upper mass limit $M_{\text{up}} = 100M_{\odot}$, which are reasonable parameters for the current star formation episode (Coppin et al. 2007; Pettini et al. 2000; Quider et al. 2009).

The strongest stellar wind feature present in the Cosmic Eye is the C IV $\lambda\lambda 1548, 1550$ P Cygni profile shown in Figure 4. Also plotted in the top panel are the two *Starburst99* model spectra for comparison. Clearly there is a good agreement between the models and the data. The main deviations from the models are due to *interstellar* Si II $\lambda 1526$ and C IV $\lambda\lambda 1548, 1550$ (see Section 4), which are evident in the blue absorption trough, and narrower intervening Al II $\lambda 1670$ and C IV $\lambda\lambda 1548, 1550$ absorption (see Section 6) which can be seen in the P Cygni emission and absorption respectively (the intervening absorptions are highlighted with

upward pointing arrows in Figure 4). Of the two model spectra shown, the one computed with libraries of Magellanic Cloud stars is the better match, while Milky Way metallicities overpredict the strength of the absorption. This conclusion is also consistent with the P Cygni profile of $N\text{V } \lambda\lambda 1238, 1242$, although the analysis of the latter is complicated by blending with the red wing of the damped $\text{Ly}\alpha$ line and some intervening absorption. Thus, we infer that $Z_{\text{O stars}} \approx 0.4 Z_{\odot}$. We also investigated the effects on the emergent P Cygni profile of varying the slope and upper mass cut-off of the IMF. As found in previous studies, (e.g. Pettini et al. 2000), there are no indications of a departure from the ‘standard’ Salpeter IMF for stars with masses $M > 5M_{\odot}$.

The lower panel of Figure 4 compares the P Cygni region of the Cosmic Eye with that of the Cosmic Horseshoe, also recorded with ESI (reproduced from Quider et al. 2009). The P Cygni profiles of these two galaxies are very similar, and both are similar to that seen in cB58 (Quider et al. 2009). The most striking difference between the Cosmic Horseshoe and the Cosmic Eye is in their interstellar absorption profiles: the Horseshoe’s interstellar absorption extends to higher outflow velocities, while in the Cosmic Eye there is strong absorption at positive velocities in $\text{Si II } \lambda 1526$ (and other ions dominant in neutral gas), as discussed above (Section 4.2). The emission component of the C IV P Cygni profile, which can be clearly seen in the Cosmic Horseshoe and cB58, seems to be absent from the Cosmic Eye. Smail et al. (2007) interpreted this as evidence that the massive stellar population of the galaxy is deficient in O-type stars; with our higher spectral resolution we can now see that the lack of emission is partly due to the presence of foreground absorption by an intervening triplet of $\text{Al II } \lambda 1670$ lines at $z_{\text{abs}} = 2.7865, 2.7891, 2.7925$ (see Table 3). Finally, nebular $\text{Si II } \lambda 1533.4312$ emission, which is evident in the Horseshoe and cB58, is weak in the Cosmic Eye.

Several blends of stellar photospheric absorption lines in the integrated spectra of star-forming galaxies have been shown to be sensitive to the metallicity of early-type stars (Leitherer et al. 2001; Rix et al. 2004). Two of these regions are a blend of $\text{Si III } \lambda 1417$, $\text{C III } \lambda 1427$, and $\text{Fe V } \lambda 1430$ absorption lines spanning the wavelength interval 1415–1435 Å (the “1425” index of Rix et al. 2004), and a blend of several Fe III absorption lines from B stars between 1935 and 2020 Å (the “1978” index). Previous work has shown the success of using the 1425 index to estimate the stellar metallicity (Rix et al. 2004; Halliday et al. 2008; Quider et al. 2009), but these same studies are divided on the effectiveness of the 1978 index.

In the case of the Cosmic Eye, we cannot use the 1425 index because it is heavily contaminated by intervening absorption lines at lower redshifts (Section 6). While these features are significantly narrower than the broad blend of stellar absorption, they nevertheless compromise the placement of the continuum in this region of the spectrum, rendering the measurement of the 1425 index too uncertain to be useful. The 1978 index region appears to be ‘clean’, but we found it to be a generally poor match to the model spectra by Rix et al. (2004), in particular being stronger than any of the metallicities considered by those authors between 1985 and 2015 Å. Quider et al. (2009) also found the 1978 index to be problematic for the Cosmic Horseshoe (although in that case the index failed between 1960 and 1980 Å), so we reiterate their cautionary note that the 1978 index needs to be tested on more galaxies to establish its usefulness as an abundance indicator.

To sum up this section, from a consideration of the C IV stellar wind profile, the population of early-type stars in the lensed galaxy of the Cosmic Eye was found to be very similar to those of the Cosmic Horseshoe and cB58 in its metallicity ($Z \sim 0.4 Z_{\odot}$), mode of

star formation (continuous), and IMF (with a Salpeter slope in the mass range $100M_{\odot} \geq M \geq 5M_{\odot}$). The 1978 index is not well-matched by the spectrum of the Cosmic Eye at any of the model metallicities, indicating that further testing of this index is necessary before it can be reliably used as a metallicity measure.

6 INTERVENING ABSORPTION SYSTEMS

Possibly because of its high redshift, and the high resolution and S/N ratio of our data, the spectrum of the Cosmic Eye shows numerous narrow absorption lines at redshifts $z < z_{\text{sys}}$ due to intervening absorbers along the line of sight. Limiting ourselves to the wavelength interval longwards of the $\text{Ly}\alpha$ line (so as to avoid the $\text{Ly}\alpha$ forest), we identified 41 such absorption lines associated with seven definite and one possible systems at redshifts from $z_{\text{abs}} = 2.4563$ to $z_{\text{abs}} = 3.0528$. Every system has a $\text{C IV } \lambda\lambda 1548, 1550$ doublet associated with it and six systems have additional low or high ionization species present. Table 3 lists the identified intervening absorption lines with their redshifts and observed equivalent widths.

Although for clarity we have labelled each resolved set of absorption lines as an ‘absorption system’, some of the absorbers are separated by redshift differences which correspond to relative velocities of only a few hundred km s^{-1} . If, for ease of comparison with earlier absorption line statistics from lower resolution work, we group together into one ‘absorption system’ lines which fall within a velocity interval $\Delta v = 1000 \text{ km s}^{-1}$, we have four such (definite) systems within a redshift interval $\Delta z = 0.81$ between $z_{\text{abs}} = 2.25$ and $z_{\text{abs}} = 3.06$, considering that we could have detected C IV doublets between $\lambda_{\text{obs}} = 5030 \text{ \AA}$ and $\lambda_{\text{obs}} = 6293 \text{ \AA}$ (approximately the redshifted wavelengths of $\text{Ly}\alpha$ and C IV in the Cosmic Eye). All four systems thus defined have $W_0(1548) \geq 0.40 \text{ \AA}$, where $W_0(1548)$ is the rest-frame equivalent width of the stronger member of the C IV doublet. Thus, in the Cosmic Eye the number of such systems per unit redshift is $N(z) = 4/0.81 \simeq 5$, or ~ 5 times higher than the mean $\langle N(z) \rangle \simeq 1$ for absorbers of this strength and in the same redshift interval in QSO spectra (Steidel 1990). It is hard to conclude, without a more detailed analysis which is beyond the scope of this paper, whether this is just a statistical fluctuation, or whether the excess number of strong C IV absorbers in front of the Cosmic Eye is at least partly due to the extension of the image on the plane of the sky (two arcs, each $\sim 3''$ long).

As can be seen in Figure 2, the intervening absorption lines are scattered throughout the spectrum of the Cosmic Eye, inconveniently falling within several features of interest. Column (5) of Table 3 details the blending of the intervening absorbers with interstellar lines in the Cosmic Eye as well as each other. There is no doubt that the presence of so many intervening absorption lines complicates the interpretation of the Cosmic Eye spectrum. This is a clear case where a high resolution spectrum reveals a more complex situation than was inferred from lower resolution observations. Thus, the Cosmic Eye serves as a cautionary tale for the interpretation of high redshift galaxy spectra which, without the boost provided by gravitational lensing, generally can only be recorded at low resolution with available instrumentation.

We also searched for $\text{Mg II } \lambda\lambda 2796, 2803$ absorption near $z = 0.73$, the redshift of the lensing galaxy of the Cosmic Eye and of at least two other galaxies in the field (Smail et al. 2007). However, these lines would fall in the $\text{Ly}\alpha$ forest and, if present, are difficult to disentangle from the intergalactic medium absorption at the S/N ratio of our data.

Table 3. INTERVENING ABSORPTION LINE SYSTEMS

λ_{obs} (Å)	Identification	z_{abs}	W_{obs} (Å)	Comments
System 1: $z_{\text{abs}} = 2.4563$				
5277.15	Si II 1526.7070	2.4567	1.31	Blended with Si IV 1393.7602 in System 4 and stellar absorption features
5351.27	C IV 1548.204	2.4564	1.80	
5360.11	C IV 1550.781	2.4564	1.26	Blended with Ni II 1317 in Cosmic Eye
5559.42	Fe II 1608.4511	2.4563	0.44	
5774.69	Al II 1670.7886	2.4563	1.88	
6409.68	Al III 1854.7184	2.4559	0.69	
6438.52	Al III 1862.7910	2.4564	0.48	
8102.21	Fe II 2344.2139	2.4563	0.85	
8235.86	Fe II 2382.7652	2.4564	1.37	
System 2: $z_{\text{abs}} = 2.6597$				
5100.64	Si IV 1393.7602	2.6596	1.08	
...	Si IV 1402.7729	Blended with Si II 1260 in Cosmic Eye
5665.89	C IV 1548.204	2.6597	1.07	
...	C IV 1550.781	Blended with Si IV 1393 in Cosmic Eye and C IV 1548 in System 3
System 3: $z_{\text{abs}} = 2.6639$				
5106.67	Si IV 1393.7602	2.6640	2.61	Blended with Si II 1253 in Cosmic Eye
...	Si IV 1402.7729	
5672.94	C IV 1548.204	2.6642	5.42	Blended with Si IV 1393 in Cosmic Eye and C IV 1550 in System 2
5682.19	C IV 1550.781	2.6641	3.64	
6794.61	Al III 1854.7184	2.6634	1.06	Blended with Al II 1670 in Cosmic Eye
System 4: $z_{\text{abs}} = 2.7865$				
5053.73	C II 1334.5323	2.7869	0.67	
5277.15	Si IV 1393.7602	2.7864	1.31	Blended with Si II 1526 in System 1 and stellar absorption features
...	Si IV 1402.7729	
5780.88	Si II 1526.7070	2.7865	0.69	Blended with O I 1302 in Cosmic Eye
5862.35	C IV 1548.204	2.7865	1.93	
5871.72	C IV 1550.781	2.7863	2.12	Blended with C IV 1548 in System 6
6090.54	Fe II 1608.4511	2.7866	0.78	
6326.42	Al II 1670.7886	2.7865	0.57	Blended with C IV P Cygni emission in Cosmic Eye
7023.16	Al III 1854.7184	2.7866	0.60	
7053.51	Al III 1862.7910	2.7865	0.34	
System 5: $z_{\text{abs}} = 2.7891$				
5057:	C II 1334.5323	2.79:	...	Blended
5281.97	Si IV 1393.7602	2.7896	0.61	Blended with stellar absorption features
...	Si IV 1402.7729	
5784.63	Si II 1526.7070	2.7890	0.83	Blended with Si II 1304 in Cosmic Eye
5866.87	C IV 1548.204	2.7895	1.45	
5876.32	C IV 1550.781	2.7893	1.00	
6330.05	Al II 1670.7886	2.7887	0.41	Blended with C IV P Cygni emission in Cosmic Eye
7026.91	Al III 1854.7184	2.7887	0.24	
7058.23	Al III 1862.7910	2.7891	0.30	
System 6: $z_{\text{abs}} = 2.7925$				
5061.13	C II 1334.5323	2.7924	1.91	
5789.76	Si II 1526.7070	2.7923	0.84	
5871.72	C IV 1548.204	2.7926	2.12	Blended with C IV 1550 in System 4
5881.45	C IV 1550.781	2.7926	0.86	
6336.16	Al II 1670.7886	2.7923	1.06	Blended with C IV P Cygni emission in Cosmic Eye
System 7: $z_{\text{abs}} = 2.8106$				
5899.50	C IV 1548.204	2.8105	1.49	
5909.52	C IV 1550.781	2.8107	1.25	
(Possible) System 8: $z_{\text{abs}} = 3.0528$				
6275.06	C IV 1548.204	3.0531	0.60	Blended with C IV P Cygni absorption in Cosmic Eye
6284.55	C IV 1550.781	3.0525	0.58	Blended with C IV P Cygni absorption in Cosmic Eye

7 DISCUSSION

One of the advantages offered by strongly lensed LBGs is that they can be observed in numerous wavebands allowing us to put together a more extensive picture of their properties than is normally possible in the absence of lensing. In this respect, the Cosmic Eye is among the better studied galaxies at $z = 3$ (see Section 2); in this section we discuss our findings from the analysis of its rest-frame UV spectrum in the light of previous work carried out at other wavelengths.

7.1 Geometry and Reddening

When Siana et al. (2009) compared the far-infrared (at wavelengths $\lambda = 40\text{--}120\ \mu\text{m}$, L_{FIR}) and UV ($1600\ \text{\AA}$, L_{1600}) luminosities of the Cosmic Eye, they found the ratio L_{FIR}/L_{1600} to be ~ 8 times lower than the value predicted with the relationship by Meurer, Heckman, & Calzetti (1999), which relates L_{FIR}/L_{1600} to the slope β of the UV stellar continuum in local starburst galaxies (assumed to be a power law of the form $F_\lambda \propto \lambda^\beta$). An analogous discrepancy, albeit by a smaller factor, was found by Siana et al. (2008) for MS 1512-cB58. These two studies attributed such departures to a steeper extinction curve for the dust in the Cosmic Eye and cB58 than that applicable to dust in local starbursts (Calzetti et al. 2000): a faster rise in the extinction A_λ with decreasing λ would have the net effect of increasing β (i.e. making the UV spectral slope redder) for a lower overall degree of dust extinction, as measured by the L_{FIR}/L_{1600} ratio. Siana et al. (2009) showed that a UV extinction curve similar to those measured in the Large and Small Magellanic Clouds could account for the observed values of L_{FIR}/L_{1600} and β in the Cosmic Eye and cB58.

The difference between the Calzetti and LMC/SMC extinction curves is thought to be one of geometry, depending on whether the bulk of the dust is mixed with, or lies in front of, the OB stars whose light is being attenuated. The implication that in cB58 and the Cosmic Eye most of the dust may be located in a ‘foreground screen’ is consistent with the finding that in both cases the UV spectra of the galaxies exhibit a damped Ly α line with near 100% covering factor (Pettini et al. 2002 for cB58, and Section 4.4 of the present paper for the Cosmic Eye). The ubiquitous presence of galaxy-scale outflows in star-forming galaxies at $z = 2 - 3$ may lead to a geometrical configuration of dust and stars more analogous to that described by the LMC/SMC curves in many LBGs, as considered by Pettini et al. (1998a). Another factor may be age: in their recent study, Reddy et al. (2010) find that it is the galaxies that are younger than ~ 100 Myr that exhibit a tendency to lie below the Meurer et al. (1999) relation.

Looking ahead, with a larger sample of high resolution spectra of strongly lensed LBGs it may be possible to disentangle the effects of geometry and age on the emergent UV flux of star-forming galaxies. An immediately obvious test is to measure the L_{FIR}/L_{1600} ratio in LBGs where the Ly α line is predominantly in emission, such as the Cosmic Horseshoe where our earlier work also showed that the interstellar medium only covers $\sim 60\%$ of the UV stellar continuum (Quider et al. 2009). In the physical picture put forward by Shapley et al. (2003) and more recently Kornei et al. (2009), the three parameters (age, Ly α luminosity, and covering factor) are related, in that galaxies with strong Ly α emission represent a later evolutionary stage, in which supernova-induced outflows have reduced the dust covering fraction.

7.2 Kinematics

The interstellar absorption lines provide information on the kinematics of the interstellar gas along our line of sight to the OB stars of the Cosmic Eye. This only allows us to make a one dimensional assessment of the gas motions in the galaxy, given that the UV light is dominated by a single source with a half-light radius of ~ 1 kpc in the lensing model of Dye et al. (2007—see Section 2). However, using laser-guided adaptive optics, Stark et al. (2008) were able to probe the two-dimensional distribution of velocities of nebular emission lines ([O III] and H β) across the face of the galaxy on unprecedented small scales of ~ 100 pc. They found a regular pattern (see Figure 2 of Stark et al. 2008) from which they constructed a rotation curve extending to ± 2 kpc from the dynamical centre with an amplitude of $v_{\text{rot}} \sin i = 55 \pm 7$ km s $^{-1}$, where i is the inclination angle. Superposed on this regular pattern are chaotic motions with a dispersion $\sigma_0 = 54 \pm 4$ km s $^{-1}$. Such a low ratio of ordered to random motions, $v_{\text{rot}}/\sigma_0 \sim 1$, is commonly found in star-forming galaxies at $z = 2\text{--}3$ (e.g. Law et al. 2009; Förster Schreiber et al. 2009).

To these kinematic data we now add measurements of outflowing gas seen in absorption. As discussed in Section 4.2, the blueshifted component of the absorption lines has maximum apparent optical depth at a velocity $v_{\text{blue}} \simeq -70$ km s $^{-1}$, relative to $z_{\text{sys}} = 3.07331$, and extends out to $v_{\text{blue}}^{\text{max}} \simeq -500$ km s $^{-1}$ (see Figure 2). In their recent analysis of outflows in low redshift starburst galaxies, Martin & Bouché (2009) associate the velocity of maximum apparent optical depth with the speed of a shell of swept-up, interstellar gas at the time of blowout from the disk of the galaxy, at a few pressure scale heights. In their picture, gas at higher negative velocities is located further away from the disk (and is therefore accelerating), and exhibits lower apparent optical depths as a result of geometrical dilution. If this scenario also applies to the Cosmic Eye, we would conclude that rotation, velocity dispersion, and outflow speed of swept-up interstellar matter at blowout are all of comparable magnitude. How all these motions fit into one coherent picture is yet far from clear, however.

It is interesting that the outflow speeds in the Cosmic Eye are lower than the values measured in most other LBGs. The value $v_{\text{blue}} \simeq -70$ km s $^{-1}$ is only about half the mean blueshift of the strongest interstellar lines in the composite spectrum of 811 LBGs constructed by Shapley et al. (2003), and lower than $v_{\text{blue}} \simeq -150$ km s $^{-1}$ and $v_{\text{blue}} \simeq -255$ km s $^{-1}$ measured in the Cosmic Horseshoe (Quider et al. 2009) and MS 1512-cB58 (Pettini et al. 2002) respectively. The maximum blueshift at which absorption is detected, $v_{\text{blue}}^{\text{max}} \simeq -500$ km s $^{-1}$ is also lower than $v_{\text{blue}}^{\text{max}} \simeq -750$ km s $^{-1}$ in both the Horseshoe and cB58. However, this limit may simply be an observational one, determined by the decrease in covering factor with distance from the central starburst, and there may be gas at higher negative velocities which is too diluted to produce detectable absorption (Martin & Bouché 2009). While there are indications at both low ($z \sim 0$, Martin 2005; Rupke et al. 2005) and intermediate ($z \simeq 1.4$, Weiner et al. 2009) redshifts that ‘superwind’ speeds scale with galactic mass and star formation rate, there is sufficient scatter in these relations to accommodate the differences we have uncovered between the three strongly lensed high- z galaxies, even though they are thought to have comparable masses and star formation rates.

Finally we note that, alongside rotation, random motions, and outflows, our UV spectrum has shown the presence of high column density, neutral gas apparently moving *towards* the OB stars in the Cosmic Eye, further complicating the kinematic picture of

this galaxy. With the available data, we cannot arrive at definite conclusions concerning the nature and location of this gas. One possibility is that it may be a chance superposition of another galaxy (or damped Ly α system) along the line of sight. Alternatively, it may be dynamically related to the Cosmic Eye. For example, it may be gas ejected from the galaxy by a previous episode of star formation and now falling back onto it, or we may be viewing a merger along a favourable sightline, although in both cases the 350 km s^{-1} velocity offset from z_{sys} seems very high, given that the Cosmic Eye does not appear to be a very massive galaxy [e.g. $M_{\text{stars+gas}} \leq 1 \times 10^{10} M_{\odot}$ (Coppin et al 2007), and $v_{\text{rot}} \sin i = 55 \text{ km s}^{-1}$ (Stark et al. 2008)]. The lensing model of Dye et al. (2007) does include a second, separate clump of UV light in the source plane, which could indicate a merger, or a foreground galaxy. However, Coppin et al. (2007) reported a redshift $z_{\text{CO}} = 3.0740 \pm 0.0002$ for the CO emission which they found to be peaked at the position of this second source; the small velocity difference $\Delta v = 50 \pm 20 \text{ km s}^{-1}$ from the systemic redshift $z_{\text{sys}} = 3.07331 \pm 0.00024$ (Section 4.1) makes it unlikely that the absorbing gas we have found with $v_{\text{red}} \simeq +350 \text{ km s}^{-1}$ is associated with the CO emitting clump.

Additional kinematic data on strongly lensed galaxies spanning a range of physical properties are clearly needed in order to explore how outflows (and in some cases presumably inflows) tie into the other motions within a galaxy, as well as the galaxy’s intrinsic characteristics.

7.3 Metallicity and Stellar Populations

The C IV P Cygni profile encodes information about the metallicity of the O stars, as well as the relative numbers of massive stars in the Cosmic Eye. Here we consider each in turn.

Up to now, the degree of metal enrichment attained by high redshift star-forming galaxies has been determined primarily from the analysis of the most prominent nebular lines emitted from their H II regions (e.g. Pettini et al. 2001; Shapley et al. 2004; Erb et al. 2006a; Maiolino et al. 2008). Strongly lensed galaxies give us the opportunity to conduct a complementary metallicity measurement based on UV spectral features due to massive stars. Young stars and H II regions are expected to have intrinsically the same chemical composition, since the former have only recently formed out of the gas which they ionize into the latter; thus a comparison between stellar and nebular abundances is essentially a consistency check which may reveal systematic offsets between different metallicity indicators. In the case of the Cosmic Eye, Stark et al. (2008) deduced a metallicity $Z_{\text{H II}} \simeq 0.9Z_{\odot}$ assuming that the upper-branch solution of the R23 method first introduced by Pagel et al. (1979) applies. On the other hand, we showed in Section 5 that at solar metallicities the C IV P Cygni profile would be stronger than observed, and that a metallicity $Z_{\text{LMC/SMC}} \approx 0.4Z_{\odot}$ gives a better match to the data. Discrepancies by factors of ~ 2 between different metallicity indicators in high redshifts galaxies are probably to be expected (Pettini 2006). On the other hand, in our earlier study of the Cosmic Horseshoe (Quider et al. 2009), we did find the metallicity deduced from the R23 index to be the odd one out (in the sense of being a factor of ~ 3 higher) among several stellar and nebular measures. At lower redshifts too, methods relying on the R23 index result in metallicities towards the upper end of the range spanned by different indicators (see, for example, Figure 2 of Kewley & Ellison 2008). In light of these considerations, the apparent difference between nebular and stellar metallicity in the Cosmic Eye is not surprising.

As mentioned in Section 5, the C IV P Cygni profiles of the Cosmic Eye, Cosmic Horseshoe, and MS 1512-cB58 are all remarkably similar. While initially this may seem to be an odd coincidence, considering that these three galaxies were randomly selected by gravitational lensing, on further reflection this result is perhaps to be expected. The key issue here is continuous star formation. When considering the composite spectrum of an entire galaxy,⁴ it is exceedingly unlikely that we would pick out a special time in its stellar evolution. While in individual regions star formation is likely to proceed in bursts, a succession of such bursts on a galaxy-wide scale will approximate a continuous process of star formation. Under such circumstances, the contrast of the C IV (and other) wind lines over the underlying OB photospheric continuum will stabilize after $\sim 50 \text{ Myr}$ from the onset of star formation, corresponding to the lifetime of the lowest mass stars contributing to the light at 1550 \AA . Since this time interval is comparable to the dynamical timescale of most LBGs (e.g. Erb et al. 2006c), only a fairly exceptional star-formation history would produce significant changes in the integrated UV stellar spectrum.

As discussed above, the stellar metallicity is also an important factor in determining the strengths of the P Cygni lines, but on this basis too we would not expect marked differences between the Cosmic Eye, the Cosmic Horseshoe and MS 1512-cB58, given that the three galaxies have similar metallicity, $Z \simeq 2/5Z_{\odot}$. Such a uniform degree of metal enrichment is in turn not as surprising as it may seem, since the three objects are of comparable luminosities, reflecting the fact that most strongly lensed galaxies targeted for detailed analyses so far are intrinsically luminous, with $L \sim L^*$. A test of these ideas would be provided by observations of highly magnified galaxies of lower intrinsic luminosity (and presumably metallicity) than the few examples studied up to now.

8 SUMMARY AND CONCLUSIONS

Strong gravitational lensing of a $z = 3.07331$ star-forming [SFR $\simeq 50 M_{\odot} \text{ yr}^{-1}$ for a Chabrier (2003) IMF] galaxy magnifies it by a factor of ~ 25 and distorts its image into two $3''$ long arcs which have been collectively named the ‘Cosmic Eye’ by their discoverers, Smail et al. (2007). The high magnification has allowed us to use the ESI spectrograph on the Keck II telescope to record the galaxy’s rest-frame UV spectrum with high resolution and S/N ratio. By analyzing these data together with existing observations of the Cosmic Eye at other wavelengths, we have reached the following main conclusions.

(i) The interstellar absorption lines exhibit two components, of approximately equal strength, which are respectively blueshifted by -70 km s^{-1} and redshifted by $+350 \text{ km s}^{-1}$ relative to the stars and H II regions. While these values apply to the gas with the highest apparent optical depths, both components include absorption spanning several hundred km s^{-1} . We associate the blueshifted component with a galaxy-wide outflow similar to, but possibly weaker than, those seen in most star-forming galaxies at $z = 2-3$. The redshifted absorption is very unusual, and may represent gas ejected by a previous episode of star formation and now falling back onto the galaxy, or a merger viewed along a favourable line of sight. Alternatively, it may just be a chance superposition of another galaxy along the line of sight.

⁴ The UV luminosity of an $L^* z = 3$ LBG is equivalent to the integrated output of $\sim 2.5 \times 10^5$ O7 stars (Pettini et al. 1998b).

(ii) Both components of the metal absorption lines show indications that they do not fully cover the OB stars against which they are being viewed; we estimate covering fractions of $\sim 70\%$ and $\sim 85\%$ for the blueshifted and redshifted component respectively. There must also be more pervasive diffuse gas, because the strong damped Ly α line, corresponding to a column density $N(\text{H I}) = (3.0 \pm 0.8) \times 10^{21} \text{ cm}^{-2}$, covers at least 95% of the UV stellar continuum. We tentatively associate this high column density of H I with the redshifted component of the metal lines, where absorption from ionized species is weak or missing altogether, and propose that it provides the ‘foreground screen’ of dust responsible for the lower-than-expected far-infrared luminosity of the Cosmic Eye found by Siana et al. (2009) with the *Spitzer Space Telescope*.

(iii) The internal kinematics of the galaxy lensed into the Cosmic Eye are very complex, our data now adding outflow, and possibly even inflow, to the rotation and velocity dispersion already known from the integral field spectroscopy with adaptive optics by Stark et al. (2008). Ordered rotation, chaotic motions, and outflow all seem to be of comparable magnitude, with $v_{\text{rot}} \sin i \approx \sigma_0 \approx v_{\text{blue}} \simeq 50\text{--}70 \text{ km s}^{-1}$. However, we do not have a model yet of how these different motions fit together into one coherent kinematic picture.

(iv) Turning to the stellar spectrum, we find that the C IV P Cygni profile is well fit by a *Starburst99* stellar population model spectrum having continuous star formation with a Salpeter IMF, stellar masses from 5 to 100 M_{\odot} , and a LMC/SMC metallicity of $Z \sim 0.4 Z_{\odot}$. The P Cygni profiles of the Cosmic Eye, the Cosmic Horseshoe, and MS 1512-cB58, three high redshift star-forming galaxies studied at high spectral resolution, are all nearly identical. This is not unexpected, however, when we consider that in each case we see the integrated light of several hundred thousand O-type stars, and that these three galaxies have similar metallicities and dynamical timescales over which star formation is taking place.

(v) The metallicity $Z \simeq 2/5 Z_{\odot}$ deduced for the O stars in the Cosmic Eye is lower by a factor of ~ 2 than the value derived from the analysis of the strong nebular lines from its H II regions using the R23 index. We consider this apparent discrepancy to reflect systematic offsets between different abundance estimators, rather than intrinsic inhomogeneities in the chemical composition of stars and ionized gas.

(vi) The interpretation of both interstellar and stellar features in the UV spectrum of the Cosmic Eye is complicated by the presence of numerous intervening absorption lines associated with eight absorption systems at redshifts $z_{\text{abs}} = 2.4563\text{--}3.0528$. These narrow features are not resolved in existing low-resolution data, highlighting the caution that should be exercised in interpreting the spectra that are typically available for unlensed LBGs.

In closing, the new data presented here further emphasize the complexity of the physical conditions which prevailed in actively star-forming galaxies at redshifts $z = 2\text{--}3$. It is remarkable that the three strongly-lensed galaxies targeted by our ESI observations, while showing very similar young stellar populations, are all different in the detailed properties of their interstellar media. Whether such variety is simply the result of different geometries and viewing angles, or has its roots in more fundamental physical reasons remains to be established. Fortunately, with the increasing attention being given to detailed studies of gravitationally lensed galaxies, we can look forward with optimism to a more comprehensive empirical picture of galaxy formation coming together in the years ahead.

ACKNOWLEDGEMENTS

We are grateful to the staff at the W. M. Keck Observatory for their competent assistance with the observations. AMQ’s research is funded by a scholarship from the Marshall Foundation, and a National Science Foundation graduate research fellowship. AES acknowledges support from the David and Lucile Packard Foundation and the Alfred P. Sloan Foundation, and CCS from NSF grant AST-0606912 and the John D. and Catherine T. MacArthur Foundation. DPS’s research is supported by the UK STFC through the award of a postdoctoral fellowship. Finally, we wish to extend thanks to those of Hawaiian ancestry on whose mountain we are privileged to be guests.

REFERENCES

- Belokurov, V., et al. 2007, *ApJL*, 671, L9
 Belokurov, V., Evans, N. W., Hewett, P. C., Moiseev, A., McMahon, R. G., Sanchez, S. F., & King, L. J. 2009, *MNRAS*, 392, 104
 Cabanac, R. A., Valls-Gabaud, D., & Lidman, C. 2008, *MNRAS*, 386, 2065
 Calzetti, D., Armus, L., Bohlin, R. C., Kinney, A. L., Koornneef, J., & Storchi-Bergmann, T. 2000, *ApJ*, 533, 682
 Chabrier, G. 2003, *PASP*, 115, 763
 Coppin, K. E. K., et al. 2007, *ApJ*, 665, 936
 Crowther, P. A., Prinja, R. K., Pettini, M., & Steidel, C. C. 2006, *MNRAS*, 368, 895
 Dye, S., Evans, N. W., Belokurov, V., Warren, S. J., & Hewett, P. 2008, *MNRAS*, 388, 384
 Dye, S., Smail, I., Swinbank, A. M., Ebeling, H., & Edge, A. C. 2007, *MNRAS*, 379, 308
 Erb, D. K., Shapley, A. E., Pettini, M., Steidel, C. C., Reddy, N. A., & Adelberger, K. L. 2006a, *ApJ*, 644, 813
 Erb, D. K., Steidel, C. C., Shapley, A. E., Pettini, M., Reddy, N. A., & Adelberger, K. L. 2006b, *ApJ*, 646, 107
 Erb, D. K., Steidel, C. C., Shapley, A. E., Pettini, M., Reddy, N. A., & Adelberger, K. L. 2006c, *ApJ*, 647, 128
 Estrada, J., et al. 2007, *ApJ*, 660, 1176
 Finkelstein, S. L., Papovich, C., Rudnick, G., Egami, E., LeFloc’h, E., Rieke, M. J., Rigby, J. R., & Willmer, C. N. A. 2009, *ApJ*, 700, 376
 Förster Schreiber, N. M., et al. 2009, *ApJ*, submitted (arXiv:0903.1872)
 Hainline, K. N., Shapley, A. E., Kornei, K. A., Pettini, M., Buckley-Geer, E., Allam, S. S., & Tucker, D. L. 2009, *ApJ*, 701, 52
 Halliday, C., et al. 2008, *A&A*, 479, 417
 Jenkins, E. B. 1971, *ApJ*, 169, 25
 Jenkins, E. B., & Tripp, T. M. 2006, *ApJ*, 637, 548
 Kennicutt, R. C., Jr. 1998, *ARA&A*, 36, 189
 Kewley, L. J., & Ellison, S. L. 2008, *ApJ*, 681, 1183
 Kornei, K. A., Shapley, A. E., Erb, D. K., Steidel, C. C., Reddy, N. A., Pettini, M., & Bogosavljević, M. 2009, *ApJ*, submitted
 Kubo, J. M., Allam, S. S., Annis, J., Buckley-Geer, E. J., Diehl, H. T., Kubik, D., Lin, H., & Tucker, D. 2009, arXiv:0812.3934
 Kudritzki, R.-P., & Puls, J. 2000, *ARA&A*, 38, 613
 Law, D. R., Steidel, C. C., Erb, D. K., Larkin, J. E., Pettini, M., Shapley, A. E., & Wright, S. A. 2009, *ApJ*, 697, 2057
 Law, D. R., Steidel, C. C., Erb, D. K., Pettini, M., Reddy, N. A., Shapley, A. E., Adelberger, K. L., & Simenc, D. J. 2007, *ApJ*, 656, 1
 Leitherer, C., et al. 1999, *ApJS*, 123, 3
 Leitherer, C., Leão, J. R. S., Heckman, T. M., Lennon, D. J., Pettini, M., & Robert, C. 2001, *ApJ*, 550, 724
 Lemoine-Busserolle, M., Contini, T., Pelló, R., Le Borgne, J.-F., Kneib, J.-P., & Lidman, C. 2003, *A&A*, 397, 839
 Lin, H., et al. 2009, *ApJ*, 699, 1242
 Maiolino, R., et al. 2008, *A&A*, 488, 463
 Martin, C. L. 2005, *ApJ*, 621, 227
 Martin, C. L., & Bouche, N. 2009, *ApJ*, in press (arXiv:0908.4271)
 Meurer, G. R., Heckman, T. M., & Calzetti, D. 1999, *ApJ*, 521, 64

- Morton, D. C. 2003, *ApJS*, 149, 205
- Noterdaeme, P., Petitjean, P., Ledoux, C., & Srianand, R. 2009, *A&A*, in press
- Ofek, E. O., Seitz, S., & Klein, F. 2008, *MNRAS*, 389, 311
- Pagel, B. E. J., Edmunds, M. G., Blackwell, D. E., Chun, M. S., & Smith, G. 1979, *MNRAS*, 189, 95
- Pettini, M. 2006 in LeBrun V., Mazure A., Arnouts S. & Burgarella D., eds., *The Fabulous Destiny of Galaxies: Bridging Past and Present*. Frontier Group, Paris, p. 319 (astro-ph/0603066).
- Pettini, M., Kellogg, M., Steidel, C. C., Dickinson, M., Adelberger, K. L., & Giavalisco, M. 1998a, *ApJ*, 508, 539
- Pettini, M., Rix, S. A., Steidel, C. C., Adelberger, K. L., Hunt, M. P., & Shapley, A. E. 2002, *ApJ*, 569, 742
- Pettini, M., Shapley, A. E., Steidel, C. C., Cuby, J.-G., Dickinson, M., Moorwood, A. F. M., Adelberger, K. L., & Giavalisco, M. 2001, *ApJ*, 554, 981
- Pettini, M., Steidel, C. C., Adelberger, K. L., Dickinson, M., & Giavalisco, M. 2000, *ApJ*, 528, 96
- Pettini, M., Steidel, C. C., Adelberger, K. L., Kellogg, M., Dickinson, M., & Giavalisco, M. 1998b, in Woodward, C. E., Shull, J. M., Thronson, H. A., eds., *ASP Conf. Ser. Vol. 148, Origins*, Astron. Soc. Pac., San Francisco, p. 67
- Pontzen, A. et al. 2010, *MNRAS*, submitted
- Quider, A. M., Pettini, M., Shapley, A. E., & Steidel, C. C. 2009, *MNRAS*, 1081, in press
- Reddy, N. A., Erb, D. K., Pettini, M., Steidel, C. C., & Shapley, A. E. 2010, *ApJ*, submitted
- Reddy, N. A., Steidel, C. C., Fadda, D., Yan, L., Pettini, M., Shapley, A. E., Erb, D. K., & Adelberger, K. L. 2006, *ApJ*, 644, 792
- Reddy, N. A., Steidel, C. C., Pettini, M., Adelberger, K. L., Shapley, A. E., Erb, D. K., & Dickinson, M. 2008, *ApJS*, 175, 48
- Rix, S. A., Pettini, M., Leitherer, C., Bresolin, F., Kudritzki, R.-P., & Steidel, C. C. 2004, *ApJ*, 615, 98
- Rupke, D. S., Veilleux, S., & Sanders, D. B. 2005, *ApJS*, 160, 115
- Salpeter, E. E. 1955, *ApJ*, 121, 161
- Seitz, S., Saglia, R. P., Bender, R., Hopp, U., Belloni, P., & Ziegler, B. 1998, *MNRAS*, 298, 945
- Shapley, A. E., Erb, D. K., Pettini, M., Steidel, C. C., & Adelberger, K. L. 2004, *ApJ*, 612, 108
- Shapley, A. E., Steidel, C. C., Pettini, M., & Adelberger, K. L. 2003, *ApJ*, 588, 65
- Shin, M.-S., Strauss, M. A., Oguri, M., Inada, N., Falco, E. E., Broadhurst, T., & Gunn, J. E. 2008, *AJ*, 136, 44
- Siana, B., et al. 2009, *ApJ*, 698, 1273
- Siana, B., Teplitz, H. I., Chary, R.-R., Colbert, J., & Frayer, D. T. 2008, *ApJ*, 689, 59
- Smail, I., et al. 2007, *ApJ*, 654, L33
- Stark, D. P., Swinbank, A. M., Ellis, R. S., Dye, S., Smail, I. R., & Richard, J. 2008, *Nature*, 455, 775
- Steidel, C. C. 1990, *ApJS*, 72, 1
- Steidel, C. C., Adelberger, K. L., Giavalisco, M., Dickinson, M., & Pettini, M. 1999, *ApJ*, 519, 1
- Steidel, C. C., Giavalisco, M., Pettini, M., Dickinson, M., & Adelberger, K. L. 1996, *ApJL*, 462, L17
- Swinbank, A. M., Bower, R. G., Smith, G. P., Wilman, R. J., Smail, I., Ellis, R. S., Morris, S. L., & Kneib, J.-P. 2007, *MNRAS*, 376, 479
- Swinbank, M., et al. 2009, *MNRAS*, in press (arXiv:0909.0111)
- Teplitz, H. I., et al. 2000, *ApJL*, 533, L65
- Vanzella, E., et al. 2009, *ApJ*, 695, 1163
- Weiner, B. J., et al. 2009, *ApJ*, 692, 187
- Wen, Z.-L., Han, J.-L., Xu, X.-Y., Jiang, Y.-Y., Guo, Z.-Q., Wang, P.-F., & Liu, F.-S. 2009, *Research in Astronomy and Astrophysics*, 9, 5
- Yuan, T.-T., & Kewley, L. J. 2009, *ApJL*, 699, L161